Nationaal Lucht- en Ruimtevaartlaboratorium
National Aerospace Laboratory NLR

Executive Summary

Computation of sound radiation from cylindrical ducts with jets using a high-order finite-volume method

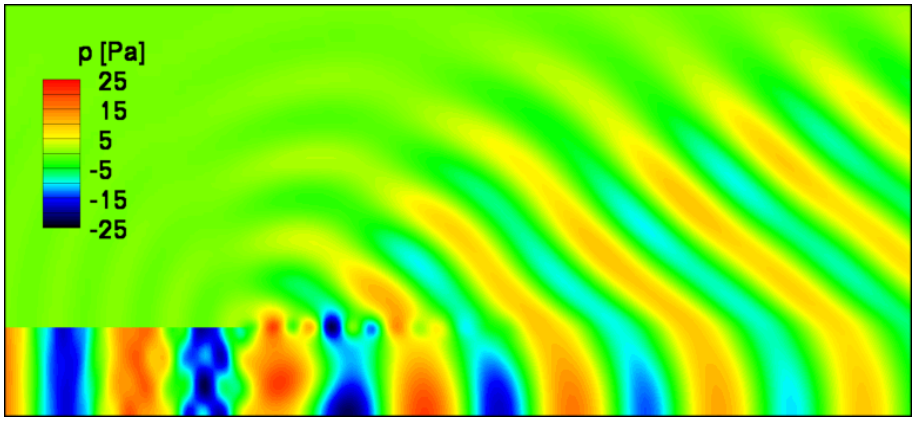

Problem area

There is a need for new concepts and technologies that reduce the noise levels of future aircraft. An important noise source on modern aircraft is the fan and turbine noise radiating from the engine exhaust. The intensity of this sound that is perceived by an observer on the ground depends on the way the sound propagates through the non-uniform flow surrounding the engine. For example, the sound may be deflected by the shear layer between the exhaust jet and the outer flow. Thus, the design of low-noise aircraft can be supported by computational methods to analyze the sound propagation through non-uniform flows. Such computations can be based on the linearized Euler equations.

Description of work

In this report, the linearized Euler equations are solved to determine the radiation of sound from cylindrical ducts carrying flow. These test cases form idealizations of the radiation of sound from engine exhaust. For these test cases, analytical solutions are available, so that the accuracy of the computational method can be verified. The linearized Euler equations are solved in the time domain using a high-order finitie-volume method. Particular attention is paid to possible instabilities of the computations along the vortex sheet between the exhaust jet and the outer flow.

Results and conclusions

Numerical solutions of the sound propagation from cylindrical ducts are presented for three flow con-

Report no.
NLR-TP-2007-514

Author(s)
J.C. Kok

Classification report
Unclassified

Date
July 2007

Knowledge area(s)
Computational Physics & Theoretical Aerodynamics
Aeroacoustics & Experimental Aerodynamics

Descriptor(s)
Engine noise
Computational aeroacoustics
High-order finite-volume method

This report is based on a presentation held at the 13th AIAA/CEAS Aeroacoustics Conference, Rome, Italy, 21-23 May, 2007.

ditions representative of different engine conditions during take-off and landing of aircraft (approach, cutback, and sideline). The sound pressure levels and the directivities of the sound in the far field compare well to the analytical solutions. Stability issues along the vortex sheet are successfully resolved by replacing the vortex sheet with a gradually spreading artificial shear layer.

Applicability
The computational method for solving the linearized Euler equations can be applied to determine the far-field directivity and intensity of tonal noise radiating from the exhaust of turbofan engines.

Nationaal Lucht- en Ruimtevaartlaboratorium, National Aerospace Laboratory NLR

Anthony Fokkerweg 2, 1059 CM Amsterdam,
P.O. Box 90502, 1006 BM Amsterdam, The Netherlands
Telephone +31 20 511 31 13, Fax +31 20 511 32 10, Web site: www.nlr.nl

Nationaal Lucht- en Ruimtevaartlaboratorium
National Aerospace Laboratory NLR

NLR-TP-2007-514

Computation of sound radiation from cylindrical ducts with jets using a high-order finite-volume method

J.C. Kok

This report is based on a presentation held at the 13th AIAA/CEAS Aeroacoustics Conference, Rome, Italy, 21-23 May, 2007.

This publication has been refereed by the Advisory Committee AEROSPACE VEHICLES.

Customer	National Aerospace Laboratory NLR
Contract number	----
Owner	National Aerospace Laboratory NLR
Division	Aerospace Vehicles
Distribution	Unlimited
Classification of title	Unclassified
	December 2007

Approved by:

Author	Reviewer	Managing department
5/3/2008	10-3-08	11/3/2008

Summary

To calculate sound radiation from the exhaust of ducts carrying flow, the linearized Euler equations are solved in the time domain with a high-order finite-volume method. The numerical solutions are compared to the analytical solutions for a hollow duct and for an annular duct with an infinite centre body. Particular attention is paid to unstable modes occurring along the vortex sheet between the uniform jet and outside flows. The computations are stabilized by replacing the vortex sheet with a gradually spreading artificial shear layer.

Contents

1 Table

13 Figures

(25 pages in total)

List of figures

This page is intentionally left blank.

1 Introduction

To determine the far-field directivity and intensity of engine fan and turbine noise radiating from exhaust nozzles, the propagation of the sound through the non-uniform flow surrounding the engine must be considered. In particular, the sound passes through the shear layer between the exhaust jet and the outer flow. Sound propagation in non-uniform flows can be computed using the linearized Euler equations. In this paper, the linearized Euler equations are solved for the radiation of sound from cylindrical ducts using a high-order finite-volume method (see Kok (Ref. 1)).

The radiation of sound from a cylindrical duct may serve as a canonical test case for the verification of numerical methods for the radiation of fan and turbine noise from exhaust nozzles. In this idealization, the mean flow field consists of two uniform flows: the jet emanating from the duct and the outer flow. The two uniform flows are separated by a vortex sheet. For the case of a semi-infinite hollow duct with subsonic jet, an analytical solution was derived by Munt (Ref. 2). This solution was used by, for example, Zhang *et al.* (Ref. 3) to verify their numerical method for the linearized Euler equations. Recently, extensions of the Munt solution were presented for an annular duct with an infinite centre body by Gabard *et al.* (Ref. 4) (acoustically hard centre body) and by Demir & Rienstra (Ref. 5) (lined centre body). Here, only the hard centre body is considered.

The linearized Euler equations are solved in the time domain for both the hollow and the annular duct using a high-order finite-volume method and the results are compared to the analytical solutions. The finite-volume method is based on the conservative form of the equations, which are discretized in space on multi-block structured grids. The method is fourth-order accurate on non-uniform, curvilinear grids, has low numerical dispersion, and has no numerical dissipation unless explicitly added. On a uniform grid, it is essentially equivalent to the DRP scheme of Tam & Webb (Ref. 6). The equations are integrated in time by the four-stage Runge–Kutta scheme. To compute the far-field sound from the near-field solution, Kirchhoff surface integration is used.

The linearized Euler equations do not only support acoustic waves, but also vorticity and entropy waves. This has as advantage that at sharp trailing edges (such as the trailing edges of the ducts) the physics can be captured correctly. At a sharp trailing edge, the fluid velocity is required to be zero (Kutta condition). An acoustic wave passing the edge induces an oscillatory non-zero velocity at the edge. To maintain the Kutta condition, a vorticity wave is generated at the trailing edge, counterbalancing the non-zero velocity due to the acoustic wave. Typically, this will lead to a vortex street downstream of the edge and this vortex street, in its turn, induces sound through pressure oscillations on the duct walls.

A disadvantage of including vorticity and entropy waves is the intrinsic instability of the vortex sheet, which forms a critical problem for numerical computations in the time domain. For computations on a sufficiently fine grid, an unstable mode is produced along the vortex sheet that grows both in space and time. As the unstable mode is not an acoustic mode, it is still possible to compute the far-field sound after a limited time interval. In practice, however, the computation may break down before the acoustic part of the solution has become sufficiently periodic.

To remove the unstable mode, one could consider modifying or simplifying the linearized Euler equations. For example, the acoustic perturbation equations could be solved (Ref. 7), excluding non-acoustic perturbations. In that case, however, the Kutta condition is not enforced at the trailing edge and therefore the sound induced by vortex shedding will be neglected. Alternatively, specific terms could be dropped from the equations (in particular, the gradient of the mean flow normal to the vortex sheet (Ref. 3)), but this does not seem to be a generally applicable approach.

In this paper, the vortex sheet is replaced by a gradually spreading artificial shear layer. This shear layer is obtained by solving the non-linear Euler equations with a second-order finite-volume method including fourth-order artificial diffusion. As shown by Michalke (Refs. 8, 9), disturbances in an inviscid shear layer will be stable provided the Strouhal number (based on the momentum thickness and the jet velocity) is large enough.

2 Model equations

To determine the near-field sound propagation, the linearized Euler equations (LEE) are solved in the time domain. In conservative form, these equations are given by

$$\frac{\partial \rho'}{\partial t} + \frac{\partial}{\partial x_j}\left(u_j \rho' + \rho u_j'\right) = 0, \tag{1a}$$

$$\frac{\partial (\rho u_i)'}{\partial t} + \frac{\partial}{\partial x_j}\left(u_j (\rho u_i)' + (\rho u_i) u_j'\right) + \frac{\partial p'}{\partial x_i} = 0, \tag{1b}$$

$$\frac{\partial (\rho E)'}{\partial t} + \frac{\partial}{\partial x_j}\left(u_j (\rho H)' + (\rho H) u_j'\right) = 0, \tag{1c}$$

with ρ the density, $\boldsymbol{u}$ the velocity vector, E the total energy per unit mass, p the pressure, and $H = E + p/\rho$ the total enthalpy per unit mass. Variables with prime represent the time-dependent perturbations; variables without prime represent the mean flow field (obtained by solving the full non-linear Euler equations or Reynolds-averaged Navier–Stokes equations). Assuming a calorically perfect gas, the pressure is given by

$$p = (\gamma - 1)\left(\rho E - \tfrac{1}{2}\rho u_i u_i\right), \tag{2}$$

with $\gamma = c_p/c_v$ the ratio of specific heats. The perturbations of conservative and primitive variables are related to each other by the following (linearized) equations:

$$(\rho \boldsymbol{u})' = \rho \boldsymbol{u}' + \boldsymbol{u}\rho', \tag{3a}$$

$$(\rho E)' = \rho E' + E\rho', \tag{3b}$$

$$p' = (\gamma - 1)\left((\rho E)' - u_i(\rho u_i)' + \tfrac{1}{2}(u_i u_i)\rho'\right), \tag{3c}$$

$$(\rho H)' = (\rho E)' + p'. \tag{3d}$$

The test cases considered here consist of sound emanating from the exhausts of cylindrical ducts. The ducts contain uniform mean flow fields leading to jets downstream of the exhaust. The acoustic field prescribed inside the duct consists of so-called duct modes, which are eigensolutions of the linearized Euler equations, containing only acoustic waves (no vorticity or entropy waves). Consider an annular cylindrical duct with outer radius R_1 and inner radius $R_2 = hR_1$ ($h < 1$). A single duct mode is given by

$$\frac{\rho'}{\rho} = \frac{p'}{\rho c^2} = \mathrm{Re}(F_{m,n}(t, x, r, \phi)), \tag{4a}$$

$$F_{m,n}(t, x, r, \phi) = A_{m,n} U_{m,n}(s) \mathrm{e}^{\mathrm{i}(\omega t - m\phi - k_{m,n} x)}, \tag{4b}$$

using cylindrical coordinates (x, r, ϕ), with c the speed of sound, $A_{m,n}$ the amplitude, ω the angular frequency, $k_{m,n}$ the axial wave number, and $U_{m,n}$ a radial eigenfunction depending on $s = r/R_1$. The mode, labelled as (m, n), is characterized by the azimuthal order $m \in \mathbb{Z}$ and the radial order $n \in \mathbb{N}^+$. The mode $(0, 1)$ is a plane wave. The velocity components in cylindrical coordinates are given by

$$\frac{u_x'}{c} = \mathrm{Re}\left(\frac{k_{m,n}}{k - M k_{m,n}} F_{m,n}\right), \tag{5a}$$

$$\frac{u_r'}{c} = \mathrm{Re}\left(\frac{\mathrm{i}}{k - M k_{m,n}} \frac{\partial F_{m,n}}{\partial r}\right), \tag{5b}$$

$$\frac{u_\phi'}{c} = \mathrm{Re}\left(\frac{m}{k - M k_{m,n}} \frac{1}{r} F_{m,n}\right), \tag{5c}$$

with wave number $k = \omega/c$ and Mach number $M = u_x/c$. The radial functions $U_{m,n}$ are eigenfunctions of the Bessel equation of order m with appropriate boundary conditions (hard walls, i.e., $u_r' = 0$ at $s = h$ and $s = 1$) and are given by

$$U_{m,n}(s) = A(J_m(\varepsilon_{m,n} s) - J_m'(\varepsilon_{m,n}) Y_m(\varepsilon_{m,n} s)/Y_m'(\varepsilon_{m,n})), \tag{6}$$

with J_m and Y_m the Bessel functions of the first and second kind and with $A > 0$ such that $\int_h^1 s U_{m,n}(s)^2 \mathrm{d}s = 1$. The eigenvalues $\varepsilon_{m,n}$ satisfy

$$Y_m'(\varepsilon_{m,n}) J_m'(\varepsilon_{m,n} h) - J_m'(\varepsilon_{m,n}) Y_m'(\varepsilon_{m,n} h) = 0 \tag{7}$$

(which follows from the boundary conditions). Only the positive eigenvalues need to be considered and are ordered such that they are increasing with n. The axial wave numbers are given by the equation

$$k_{m,n}^2 - (k - Mk_{m,n})^2 + \alpha_{m,n}^2 = 0, \tag{8}$$

with $\alpha_{m,n} = \varepsilon_{m,n}/R_1$ and with the solutions

$$k_{m,n}^{\pm} = \frac{-Mk \pm \xi_{m,n}}{\beta^2} \tag{9}$$

where $\beta^2 = 1 - M^2$ and

$$\xi_{m,n} = \begin{cases} \sqrt{k^2 - \beta^2\alpha_{m,n}^2} & , \quad |\beta\alpha_{m,n}| \le |k| \\ -\mathrm{i}\sqrt{\beta^2\alpha_{m,n}^2 - k^2} & , \quad |\beta\alpha_{m,n}| \ge |k| \end{cases}. \tag{10}$$

For $k_{m,n} = k_{m,n}^+$ the mode travels downstream (assuming $u_x > 0$), whereas for $k_{m,n} = k_{m,n}^-$ the mode travels upstream. The mode is called cut-on if the axial wave number $k_{m,n}$ is real, i.e., if $|\beta\alpha_{m,n}| \le |k|$, and it is called cut-off otherwise. Finally, the acoustic intensity or energy flux in axial direction I is defined as

$$\frac{I}{\rho c^3} = \frac{(\rho u_x)' H'}{\rho c^3} = \left(\frac{u_x'}{c} + M\frac{\rho'}{\rho}\right)\left(\frac{\rho'}{\rho} + M\frac{u_x'}{c}\right). \tag{11}$$

Averaged over one time period and over the duct cross section, the intensity of one duct mode travelling downstream is given by

$$\frac{\langle I\rangle}{\rho c^3} = \frac{A_{m,n}^2}{1 - h^2}\frac{k\xi_{m,n}}{(k - Mk_{m,n})^2}. \tag{12}$$

If the intensity is given, this defines the amplitude $A_{m,n}$ of the mode.

The linearized Euler equations are solved to determine the acoustic field in the region where the mean flow is not uniform. To determine the far-field sound from this near-field solution, a Kirchhoff surface integral is employed, formulated in the Fourier domain. Consider an integration surface S enclosing the duct and the jet. Outside this surface the mean flow field is uniform. The Kirchhoff formulation of Farassat(Ref. 10) gives the solution of the wave equation in an observer point $\boldsymbol{x}$ outside a moving, closed surface S, given the solution on the surface. Here, however, the solution of the wave equation in a uniform flow is required, while the surface S is stationary. This solution is obtained by letting the surface and the observer in Farassat's formulation move with a constant velocity equal but opposite to the velocity $\boldsymbol{u}$ of the uniform flow. After Fourier transformation in time, one then finds the following integral formulation. Given the Fourier

transform of the pressure perturbation $\hat{p}$ and its gradient $\nabla\hat{p}$ on the surface S (obtained from the LEE solution), the Fourier transform of the pressure perturbation field outside S at angular frequency ω is given by

$$\hat{p}(\boldsymbol{x},\omega) = \int_{\boldsymbol{y}\in S} \frac{1}{R}\left((M_n\boldsymbol{M}-\boldsymbol{n})\cdot\nabla\hat{p} + \mathrm{i}k\left(M_n + \frac{r_n}{R}\right)\hat{p} + \beta^2\frac{r_n}{R^2}\hat{p}\right)\mathrm{e}^{-\mathrm{i}kr^*}\,\mathrm{d}S, \qquad (13)$$

with $\boldsymbol{n}$ the outward unit normal on S, $k = \omega/c$ the wave number, $\boldsymbol{M} = \boldsymbol{u}/c$ the Mach vector, $M_n = \boldsymbol{M}\cdot\boldsymbol{n}$, $\beta^2 = 1 - M^2$, $\boldsymbol{r} = \boldsymbol{x} - \boldsymbol{y}$, $r = \|\boldsymbol{r}\|$, $r_n = \boldsymbol{r}\cdot\boldsymbol{n}$, $R = \sqrt{(\boldsymbol{M}\cdot\boldsymbol{r})^2 + \beta^2 r^2}$, and $r^* = (R - \boldsymbol{M}\cdot\boldsymbol{r})/\beta^2$.

Given the pressure perturbation in the far field, the (overall) sound pressure level is defined by

$$\mathrm{SPL}(\boldsymbol{x}) = 20\log\left(\frac{\|p'(\boldsymbol{x})\|}{p_{\mathrm{ref}}}\right), \qquad (14)$$

with $\|p'\|$ the RMS value of p' in time and with $p_{\mathrm{ref}} = 2\cdot 10^{-5}\,\mathrm{Pa}$.

3 Numerical method

The conservative linearized Euler equations are discretized on multi-block structured grids using a cell-centred, finite-volume method. The method is fourth-order accurate on non-uniform, curvilinear grids and has low numerical dispersion. The fourth-order accuracy has been obtained by extending the approach of Verstappen & Veldman (Ref. 11), which uses Richardson extrapolation, from Cartesian grids to curvilinear grids. The low dispersion has been obtained by extending the DRP scheme of Tam & Webb (Ref. 6) to finite-volume methods. A small amount of sixth-order numerical diffusion is added to ensure stability. The equations are integrated in time with the standard four-stage Runge–Kutta scheme. The method is summarized here; details of its derivation can be found in Kok (Ref. 1).

For each cell centre, consider two control volumes: the control volume Ω^h consisting of one grid cell (with mesh size h in the computational domain) and the control volume Ω^{3h} consisting of three grid cells in each direction (with mesh size $3h$ in the computational domain), as illustrated in figure 1 in 2D. For both control volumes, the same second-order finite-volume scheme is applied. Combining the schemes with Richardson extrapolation in order to cancel the leading-order error results in a fourth-order accurate finite-volume scheme, given by

$$\frac{\mathrm{d}U_{i,j,k}}{\mathrm{d}t} + \frac{B_{i,j,k}}{V_{i,j,k}} = 0, \qquad (15)$$

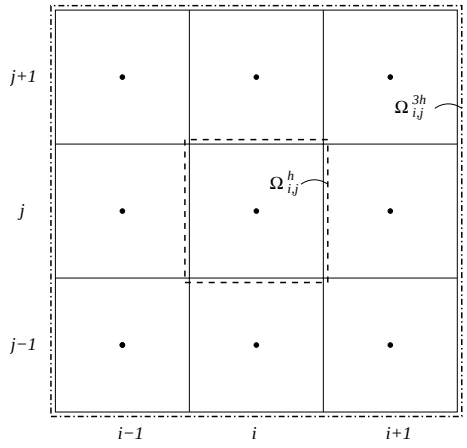

Fig. 1 Control volumes $\Omega_{i,j}^{h}$ and $\Omega_{i,j}^{3h}$ around cell centre (i,j) in 2D.

with U the vector of dependent variables, B the flux balance, V the grid-cell volume, and (i,j,k) the grid-cell indices. The high-order flux balance and cell volume are given by

$$B_{i,j,k} = \frac{9}{8} B_{i,j,k}^{h} - \frac{1}{8 \cdot 3^{d}} B_{i,j,k}^{3h}, \tag{16a}$$

$$V_{i,j,k} = \frac{9}{8} V_{i,j,k}^{h} - \frac{1}{8 \cdot 3^{d}} V_{i,j,k}^{3h}, \tag{16b}$$

with d the spatial dimension and with superscripts h and $3h$ indicating the respective control volumes. The balance $B_{i,j,k}^{h}$ involves, for example, the flux $F_{i+1/2,j,k}^{h}$ between control volumes $\Omega_{i,j,k}^{h}$ and $\Omega_{i+1,j,k}^{h}$, whereas the balance $B_{i,j,k}^{3h}$ involves the flux $F_{i+3/2,j,k}^{3h}$ between control volumes $\Omega_{i,j,k}^{3h}$ and $\Omega_{i+3,j,k}^{3h}$. In the basic fourth-order scheme, these fluxes are computed by averaging the dependent variables from the appropriate cell centres. A fourth-order scheme with low dispersion is obtained by computing the fluxes from the following extended averages:

$$U_{i+1/2,j,k}^{h} = \frac{1-\alpha}{2} \left(U_{i,j,k} + U_{i+1,j,k} \right) + \frac{\alpha}{2} \left(U_{i-1,j,k} + U_{i+2,j,k} \right), \tag{17a}$$

$$U_{i+3/2,j,k}^{3h} = \frac{1-\beta}{2} \left(U_{i,j,k} + U_{i+3,j,k} \right) + \frac{\beta}{2} \left(U_{i+1,j,k} + U_{i+2,j,k} \right). \tag{17b}$$

(The basic fourth-order scheme is recovered for $\alpha = \beta = 0$.) Fourth-order accuracy requires that

$$\alpha = -\tfrac{1}{9}\beta. \tag{18}$$

In order to minimize the dispersion of the scheme, the coefficient β is chosen such that the scheme is equivalent to the finite-difference DRP scheme of Tam & Webb on a uniform, Cartesian grid. This is the case if

$$\beta = -2.00047085298. \tag{19}$$

The discretization is based on the full 3D equations. For the test cases considered here, the geometry and the mean flow field are axisymmetric and the sound field is periodic in the azimuthal direction if one duct mode is considered. Thus, essentially a 2D problem can be solved per duct mode. Zhang *et al.* (Ref. 3) derive a particular 2D form (or 2.5D as they call it) of the linearized Euler equations for this situation in cylindrical coordinates, using the known frequency and azimuthal order of the considered duct mode. These equations, however, are not in conservative form and are therefore not suitable for a finite-volume method. Nevertheless, it is not necessary to solve the full 3D problem. Consider an axisymmetric grid. From this grid, only two layers of grid cells in the azimuthal direction are used (forming a segment of typically 0.2°). Together with the azimuthal order, the solution in these two layers is sufficient to determine the dependence of the solution on the azimuth. This allows one to set the solution in ghost cells outside the considered segment. Finally, these ghost-cell values are used in the discretized equations defined for the two grid-cell layers.

At the upstream boundary inside the duct, an incident duct mode travelling downstream is given as boundary condition. Reflections of waves leaving the domain at this boundary may spoil the solution. In order to reduce these reflections, a buffer zone is defined adjacent to the boundary (see, e.g., Richards *et al.* (Ref. 12)). In this zone, a forcing function is added to the linearized Euler equations that forces the solution towards the incident duct mode. The forcing function (added to the left-hand side of equation (15)) is given by

$$\frac{\sigma(d)}{\tau}(U_{i,j,k} - U_p), \tag{20}$$

with U_p the prescribed duct mode, τ an appropriate time scale taken as $\tau = l_b/c$, and l_b the width of the buffer zone. The damping coefficient is defined as a function of the distance d from the inner (or down-stream) boundary of the buffer zone as follows:

$$\sigma(d) = \sigma_1 \left(\min \left\{ \frac{d}{l_b}, 1 \right\} \right)^2, \tag{21}$$

with the damping going smoothly to zero as the inner boundary of the buffer zone is approached. For all presented computations, a coefficient $\sigma_1 = 10$ has been used.

At other inflow and outflow boundaries, boundary conditions based on one-dimensional characteristic theory are applied. As these boundary conditions are not perfectly non-reflecting, buffer zones are also placed adjacent to these boundaries. The same forcing function as above is used, but with $U_p \equiv 0$.

The solid walls are considered as acoustically hard. Thus, a slip boundary conditions is applied (normal velocity component equal to zero).

The equations are integrated in time until a time-periodic solution is reached, where the time period is determined by the frequency of the incident duct mode. The computations are started from an acoustic field identical to zero. Thus, initially there is a discontinuity at the upstream boundary inside the duct between the incident duct mode and the zero acoustic field. This discontinuity gives rise to spurious waves of different frequencies and wave numbers. These spurious waves are damped by the buffer zones. For the computations for the duct mode $(0, 1)$ (plane wave), these spurious waves are the most pronounced. To improve the convergence towards the time-periodic solution for this mode, the acoustic field after every time period is averaged with the field from one time period earlier. This will damp all waves with frequencies that are not multiples of the frequency of the incident mode.

4 Annular and hollow duct

Two types of semi-infinite cylindrical ducts are considered: a hollow, circular duct (Fig. 2) and an annular duct with an infinite centre body (Fig. 3), both with an outer radius $R_1 = 1.212\,\mathrm{m}$ and with a radius $R_2 = 0.947\,\mathrm{m}$ for the centre body. The free-stream and duct flows are both uniform, with the duct flow continuing downstream from the duct exits as uniform jet. A vortex sheet separates the free-stream and jet flows.

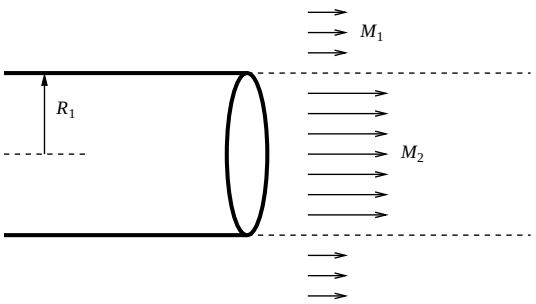

Fig. 2 Hollow duct

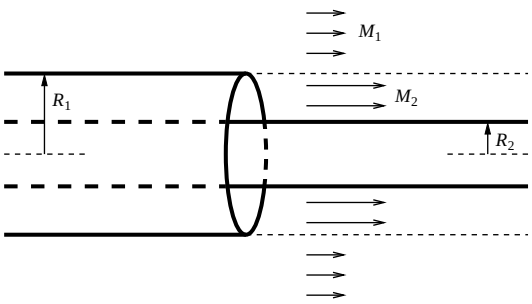

Fig. 3 Annular duct

Two flow conditions are defined, considered representative of a bypass duct at cutback and sideline engine conditions. These conditions are given in table 1, together with the frequency used for the incident duct modes (fan blade passing frequency). Incident duct modes are prescribed with different azimuthal orders (m) and the first radial order ($n = 1$). The amplitude of the duct modes is such that the intensity $\langle I \rangle = 1\,\mathrm{W/m^2}$.

4.1 Computational set-up

Grids should be defined that are fine enough to avoid excessive dispersion and dissipation of the acoustic waves. The high-order finite-volume method requires at least eight grid cells per wave

Table 1 Flow conditions and blade passing frequency (BPF) for different engine conditions (Mach number, total pressure, and total temperature for free-stream (1) and duct (2) flows)

	Cutback	Sideline
M_1	0.269	0.265
$T_{\text{tot},1}$ (K)	292.17	292.04
$p_{\text{tot},1}$ (Pa)	106551	106394
M_2	0.737	0.861
$T_{\text{tot},2}$ (K)	336.68	348.56
$p_{\text{tot},2}$ (Pa)	145370	164385
Fan BPF (Hz)	1430	1580
Fan kR_1	31.17	34.45

length (similar to the DRP scheme). Three levels of grid resolution are considered with at least the medium level satisfying this requirement. The fine level is used to check whether the numerical solutions are grid converged. The medium and coarse levels are obtained from the fine level by coarsening with a factor 2 and 4 in each computational direction.

For both ducts, 2-block grids are used with one block inside the duct and jet and one block outside. See figure 4 for an impression. For the annular duct, the block inside the duct and jet has 320×32 cells of which 128×32 cells inside the duct. The block outside the duct has 384×96 cells. The grid is uniform for $x \in [-1.6\,\text{m}, 3.2\,\text{m}]$ and $r \in [0.947\,\text{m}, 1.477\,\text{m}]$, with a mesh size $\Delta x = 0.0125\,\text{m}$. Outside the uniform region, the grid is stretched to the outer boundary at $10R_1$ from the duct exit.

For the hollow duct, the block inside the duct and jet contains more grid cells: 352×64 of which 96×64 inside the duct. The block outside the duct has 416×96 cells. The grid is uniform in a larger region then for the annular duct, with $x \in [-1.818\,\text{m}, 3.636\,\text{m}]$ and $r \in [0.0\,\text{m}, 1.818\,\text{m}]$ and with a mesh size $\Delta x = 0.0189\,\text{m}$. The same outer boundary is used as for the annular duct.

Per time period, at least 64 time steps are taken on the fine grid level, with a maximum CFL number equal to 0.53 (CFL $= (u_x + c)\Delta t/\Delta x$). On the medium and coarse levels, the same CFL numbers are used. For the hollow duct, more than 64 time steps are needed for the incident duct modes with $m > 0$ in order to avoid instabilities along the singular line $r = 0$, where the mesh size in azimuthal direction goes to zero.

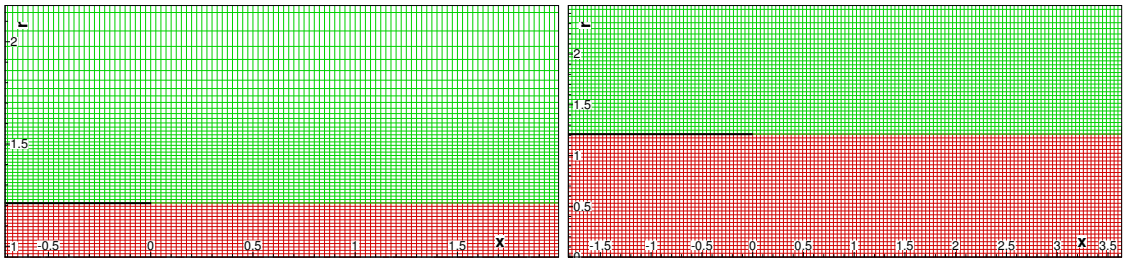

(a) Annular duct *(b) Hollow duct*

Fig. 4 Near-field grid for circular ducts at medium grid level (i.e., coarsened by factor two)

As Kirchhoff surface, a cylinder is used that extends in up and down-stream directions to the outer boundary of the grid. It has a radius $r = 1.345\,\mathrm{m}$ for the annular duct and $r = 1.515\,\mathrm{m}$ for the hollow duct.

4.2 Instability of vortex sheet

Initially, computations were performed for the annular duct using the uniform free-stream and duct flows separated by a vortex sheet as mean flow field. On the fine grid, however, an unstable mode was produced along the vortex sheet in the computations. This mode, which grows both in space and time, is illustrated in figure 5a (cutback condition, mode $(0, 1)$). The production of such a mode is consistent with the intrinsic instability of the vortex sheet. As the unstable mode is not an acoustic mode, it is still possible to compute the far-field sound by Kirchhoff integration, if it is based on the solution after a limited time interval. In order to be able to continue the computations for longer time periods, however, it is desirable to stabilize this mode.

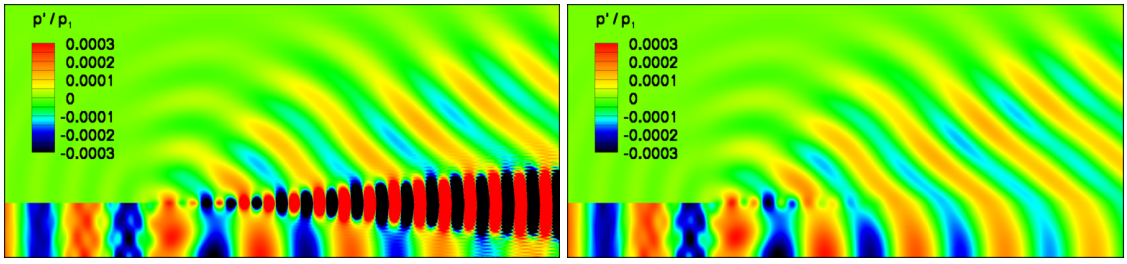

(a) Unstable mode using vortex sheet as mean flow *(b) Stabilized solution using artificial shear layer as mean flow*

Fig. 5 Annular duct: Near-field pressure perturbation (dimensionless) for unstable and stabilized computations (cutback condition, mode (0,1))

To remove the unstable mode, the vortex sheet is replaced by a gradually spreading artificial shear layer. As shown by Michalke (Refs. 8, 9), disturbances in an inviscid shear layer will be

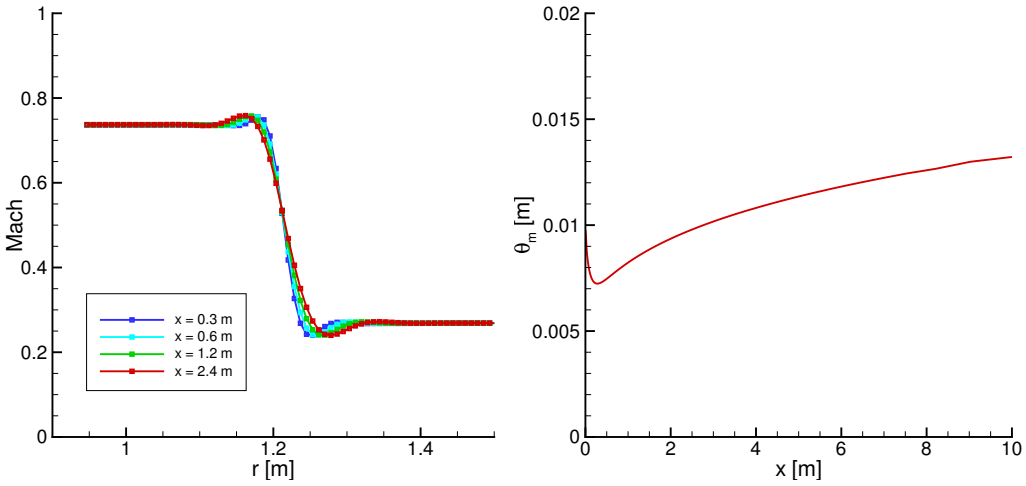

(a) Mach number at several sections *(b) Momentum thickness*

Fig. 6 Annular duct: Artificial shear layer

stable provided the frequency is large enough. For an incompressible, isothermal, parallel shear layer between a jet and a fluid at rest, the angular frequency ω of the disturbance should satisfy

$$\frac{\omega\theta_m}{U_0} > 0.25, \tag{22}$$

with θ_m the (incompressible) momentum thickness of the shear layer and U_0 the the jet velocity, provided the shear layer is thin ($\theta_m < 0.08R$ with R the jet radius). This criterion is only taken as an indication here, as a compressible flow with a heated jet and a non-zero free stream is considered. Michalke (Ref. 9) indicates that the effect of both compressibility and temperature is to reduce the frequency range of unstable modes, whereas the effect of a free stream is to increase this range (at least for a thick shear layer with $\theta_m = 0.2R$). Using the frequency of the incoming duct mode ($f = 1430\,\mathrm{Hz}$) and taking the velocity scale equal to the difference of the jet and free-stream velocities ($U_0 = 166\,\mathrm{m/s}$), the stability criterion in terms of the momentum thickness becomes

$$\theta_m > 4.6\,\mathrm{mm}. \tag{23}$$

The artificial shear layer is obtained by solving the non-linear Euler equations with a second-order finite-volume method including fourth-order artificial diffusion (on the same grid as used for the LEE computations). This artificial shear layer is illustrated in figure 6 in terms of the Mach-number profile and the (incompressible) momentum thickness. Clearly, the momentum thickness satisfies the stability criterion given above. Note that the velocity profile is non-monotonic due to the fact that the artificial diffusion is of fourth order. It is stressed that this artificial

shear layer should not be compared to a physical shear layer. Its only purpose is to stabilize the acoustic computations; not to model a physical shear layer.

The LEE solution obtained with the artificial shear layer as mean flow is shown in figure 5b. The mode that was unstable is still present, but no longer grows in space or time. The far-field sound pressure levels (SPL), computed from the unstable and stabilized solutions, are shown in figure 7. Only small differences can be seen. Thus, the artificial shear layer is thin enough to keep the far-field sound essentially unchanged, allowing comparison to the analytical solutions, while it is thick enough to stabilize the computations. All results presented in the remainder of this paper have been obtained using the artificial shear layer.

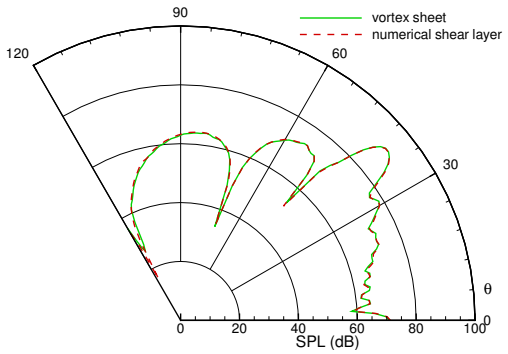

Fig. 7 Annular duct: Far-field sound-pressure level (SPL) computed using either vortex sheet or artificial shear layer as mean flow (cutback condition, mode (0,1))

4.3 Results

Computations have been performed for both flow conditions and for a selection of incident modes, with the azimuthal order m ranging from 0 (plane wave) to values close to the cut-off boundary (and with the radial order $n = 1$). All these computations were found to be stable. In figures 8 to 13, a selection of near-field and far-field solutions as obtained after a time length of 30 to 60 periods is presented. The near-field solutions show how the incident duct mode is scattered into different radial modes a the duct exit, some of which are reflected back into the duct. The far-field solution is given in terms of the sound-pressure level (SPL). It is plotted at a distance of $46\,\mathrm{m}$ from the centre of the duct exit and as a function of the polar angle θ.

Overall, the dependence of the solutions on the grid level is weak. Typically, the difference between the medium-grid and fine-grid solutions is only very small and the fine-grid solution can be considered grid converged. For the hollow duct, the grid dependence is slightly stronger due to the slightly larger mesh sizes.

The numerical solutions are compared to analytical solutions. These analytical solutions (extended Munt solutions) have been obtained by Demir & Rienstra(Ref. 5) with and without enforcing the Kutta condition at the trailing edges of the ducts. Comparisons to the solutions including the Kutta condition are made as this condition is effectively also part of the linearized Euler equations.

Generally, the computed solutions compare well to the analytical solutions. The largest differences with the analytical solutions are seen for directivity angles between 0 and 30 degrees. This is the strongest for mode (0,1) (plane wave, Figs. 8 and 10), in particular for the hollow duct. The near-field solutions show that in these cases there are strong waves travelling inside the jet. To compute the far-field sound more accurately, these waves have to be captured over a longer distance, which requires extending the uniform-grid region further downstream. For higher spinning modes, generally, there are no such waves travelling inside the jet and most sound is radiated sideways. In those cases, good agreement is found between the numerical and analytical solutions (Figs 9, 11, and 12). An exception is shown in Fig. 13 for mode $(48, 1)$ (sideline condition). In this case, there is also a wave travelling in the jet, but this time it appears to be fully captured inside the jet. Thus, most sound energy does not reach the far field, as is consistently shown by both the analytical and the numerical solutions.

5 Conclusion

A high-order, finite-volume scheme for the linearized Euler equations has been applied successfully to the computation of sound propagation from cylindrical ducts. Consistent with the Kelvin–Helmholtz instability, the computations reveal an unstable mode if the mean flow field consists of a jet and outer flow separated by a vortex sheet. The computations are stabilized by replacing the vortex sheet by a gradually spreading, artificial shear layer. This shear layer is found to be thin enough to leave the far-field solution unchanged. The numerical solutions compare well to analytical solutions for a hollow duct and for an annular duct with an infinite centre body, in particular for higher spinning modes. If the incident mode is a plane wave, then accurate computation of the far-field sound at small directivity angles is made more difficult due to strong waves travelling inside the jet, requiring a uniform grid extending far downstream.

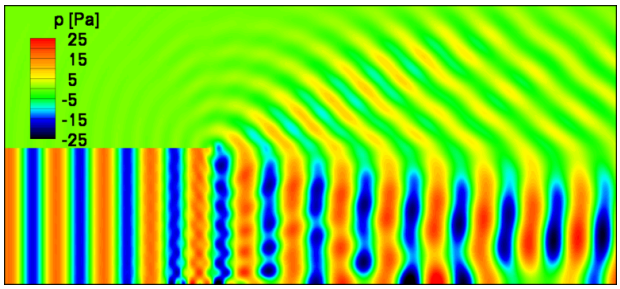

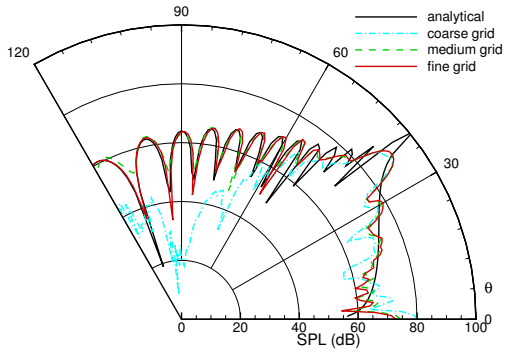

(a) Near-field pressure perturbation *(b) Far-field sound-pressure level (SPL)*

Fig. 8 Hollow duct: Cutback condition, mode (0,1)

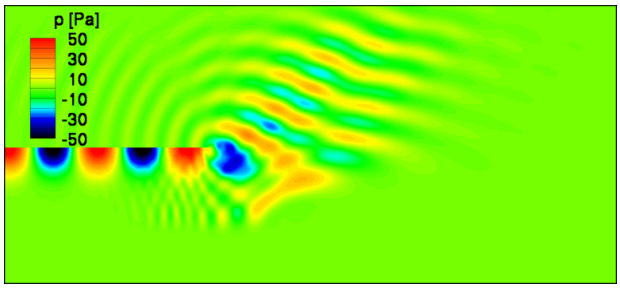

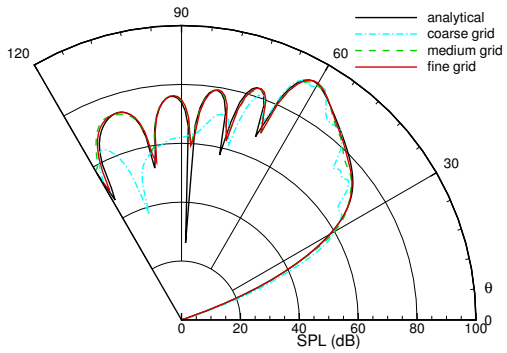

(a) Near-field pressure perturbation *(b) Far-field sound-pressure level (SPL)*

Fig. 9 Hollow duct: Cutback condition, mode (20,1)

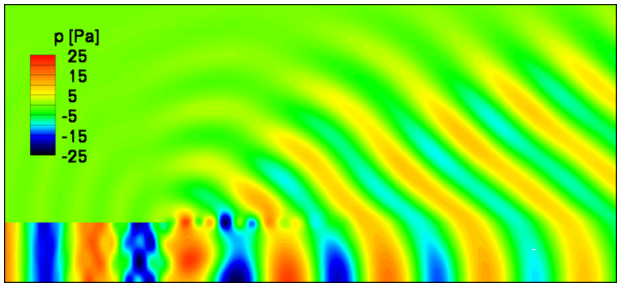

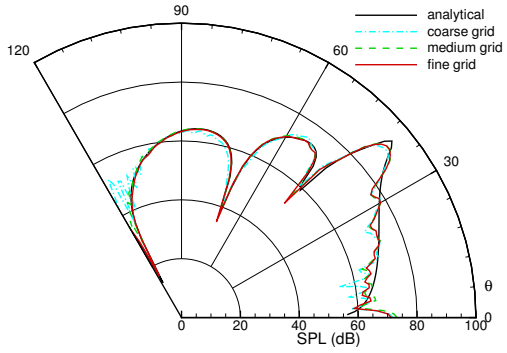

(a) Near-field pressure perturbation *(b) Far-field sound-pressure level (SPL)*

Fig. 10 Annular duct: Cutback condition, mode (0,1)

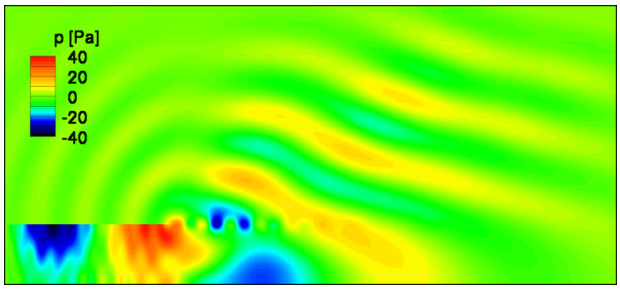

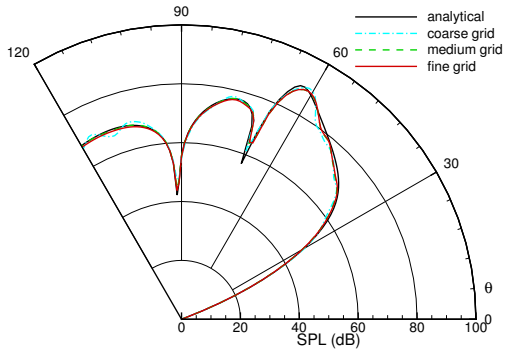

(a) Near-field pressure perturbation *(b) Far-field sound-pressure level (SPL)*

Fig. 11 Annular duct: Cutback condition, mode (21,1)

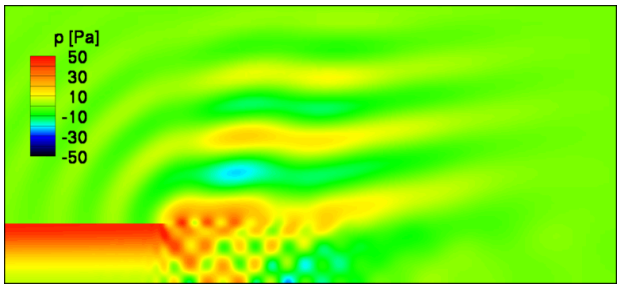

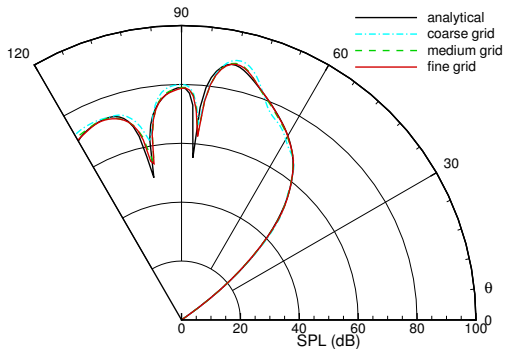

(a) Near-field pressure perturbation *(b) Far-field sound-pressure level (SPL)*

Fig. 12 Annular duct: Sideline condition, mode (32,1)

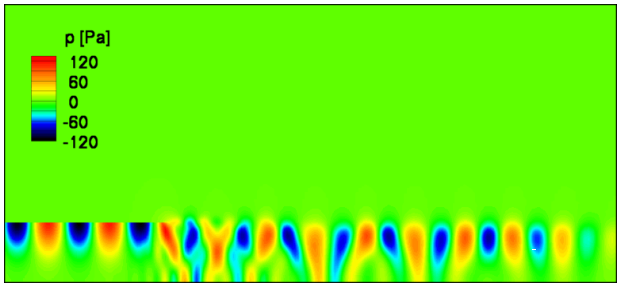

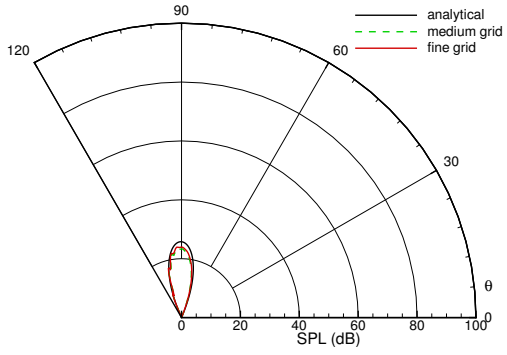

(a) Near-field pressure perturbation *(b) Far-field sound-pressure level (SPL)*

Fig. 13 Annular duct: Sideline condition, mode (48,1)

Acknowledgments

This work was partially performed within the EU project TURNEX (Turbomachinery Noise Radiation through the Engine Exhaust), which is funded by the European Union under Contract No. AST4-CT-2005-516079 of the European Commission, and partly within NLR's Programmatic Funding.

The analytical solutions were kindly provided by Ahmet Demir and Sjoerd Rienstra (TU Eindhoven).

References

1. Kok, J. C., "A Symmetry and Dispersion-Relation Preserving High-Order Scheme for Aeroacoustics and Aerodynamics," *ECCOMAS CFD 2006*, edited by P. Wesseling, E. Oñate, and J. Périaux, Egmond aan Zee, The Netherlands, 5–8 September 2006, NLR-TP-2006-525.
2. Munt, R. M., "The Interaction of Sound with a Subsonic Jet Issuing from a Semi-Infinite Cylindrical Pipe," *Journal of Fluid Mechanics*, Vol. 83, No. 4, 1977, pp. 609–640.
3. Zhang, X., Chen, X. X., and Morfey, C. L., "Acoustic Radiation from a Semi-Infinite Duct with a Subsonic Jet," *International Journal of Aeroacoustics*, Vol. 4, No. 1-2, 2005, pp. 169–184.
4. Gabard, G. and Astley, R. J., "Theoretical Models for Sound Radiation from Annular Jet Pipes: Far- and Near-Field Solutions," *Journal of Fluid Mechanics*, Vol. 549, 2006, pp. 315–342.
5. Demir, A. and Rienstra, S. W., "Sound Radiation from an Annular Duct with Jet Flow and a Lined Centerbody," *12th AIAA/CEAS Aeroacoustics Conference*, Cambridge, MA, USA, 8-10 May 2006, AIAA Paper 2006-2718.
6. Tam, C. K. W. and Webb, J. C., "Dispersion-Relation-Preserving Finite Difference Schemes for Computational Acoustics," *Journal of Computational Physics*, Vol. 107, 1993, pp. 262–281.
7. Huang, X., Ma, Z., and Zhang, X., "Computation of Modal Radiation Through an Engine Exhaust on Adaptively Refined Meshes," *ECCOMAS CFD 2006*, edited by P. Wesseling, E. Oñate, and J. Périaux, Egmond aan Zee, The Netherlands, 5–8 September 2006.
8. Michalke, A., "On Spatially Growing Disturbances in an Inviscid Shear Layer," *Journal of Fluid Mechanics*, Vol. 23, No. 3, 1965, pp. 521–544.
9. Michalke, A., "Survey on Jet Instability Theory," *Progress in Aerospace Sciences*, Vol. 21, 1984, pp. 159–199.
10. Farassat, F. and Myers, M. K., "Extension of Kirchhoff's Formula to Radiation from Moving Surfaces," *Journal of Sound and Vibration*, Vol. 123, No. 3, 1988, pp. 451–460.
11. Verstappen, R. W. C. P. and Veldman, A. E. P., "Symmetry-Preserving Discretization of Turbulent Flow," *Journal of Computational Physics*, Vol. 187, No. 1, 2003, pp. 343–368.
12. Richards, S. K., Zhang, X., Chen, X. X., and Nelson, P. A., "The Evaluation of Non-Reflecting Boundary Conditions for Duct Acoustic Computation," *Journal of Sound and Vibration*, Vol. 270, No. 3, 2004, pp. 539–557.